APPLIED PHYSICS LETTERS 102, 233303 (2013)

Contact properties of high-mobility, air-stable, low-voltage organic n-channel thin-film transistors based on a naphthalene tetracarboxylic diimide

R. Rödel,[1,a)] F. Letzkus,[2] T. Zaki,[2,3] J. N. Burghartz,[2,3] U. Kraft,[1] U. Zschieschang,[1] K. Kern,[1,4] and H. Klauk[1]

[1]Max Planck Institute for Solid State Research, Heisenbergstr. 1, 70569 Stuttgart, Germany
[2]Institute for Microelectronics Stuttgart (IMS CHIPS), Allmandring 30a, 70569 Stuttgart, Germany
[3]Institute for Nano- and Microelectronic Systems (INES), University of Stuttgart, 70569 Stuttgart, Germany
[4]Institut de Physique de la Matière Condensée, Ècole Polytechnique Fédérale de Lausanne, 1015 Lausanne, Switzerland

(Received 19 April 2013; accepted 28 May 2013; published online 12 June 2013)

Air-stable bottom-gate, top-contact n-channel organic transistors based on a naphthalene diimide exhibiting electron mobilities up to 0.8 cm^2/Vs at low voltages were fabricated. Transistors with channel lengths of 1 μm show a transconductance of 60 mS/m, but are significantly limited by the contact resistance. Transmission line measurements in combination with contact resistance models were applied to investigate this influence. Both contact resistance and contact resistivity are proportional to the inverse gate overdrive voltage. Organic complementary ring oscillators were fabricated on a flexible plastic substrate showing record signal delays down to 17 μs at a supply voltage of 2.6 V. © *2013 AIP Publishing LLC*. [http://dx.doi.org/10.1063/1.4811127]

Organic thin film transistors (TFTs) are useful for flexible, large-area electronics.[1–5] For many of these applications, the TFTs should be able to operate at low voltages and have large field-effect mobility, negligible contact resistance, good air stability, and high switching speed. One possibility to increase the switching speed is to reduce the intrinsic and parasitic device capacitances by minimizing the lateral dimensions (channel length and overlap between gate electrode and source/drain contacts). However, at small dimensions, parasitic resistances at the source/drain contacts can become dominant, necessitating a careful analysis of the contact properties.

For organic p-channel TFTs, these requirements have been met with good results.[6,7] To benefit from the advantages of complementary circuits (low static power dissipation, large noise margins), organic n-channel transistors with similar performance are needed as well.

The frequency limit of organic TFTs is usually extracted from the signal delay of ring oscillators. For organic complementary ring oscillators, stage delays below 1 μs have been reported.[8,9] However, these circuits required high voltages ($\geq$ 20 V) and an inert atmosphere, due to the lack of air stability of the C_{60} n-channel TFTs. Ambient operation of organic complementary circuits is possible with n-channel TFTs based on $F_{16}CuPc$[10] that show excellent air stability,[11] but poor electron mobility (0.05 cm^2/Vs).

Recently, air-stable n-channel TFTs based on high-mobility naphthalene and perylene derivatives have been demonstrated.[12–17] Here, n-channel TFTs based on N,N′-bis-(heptafluorobutyl)-2,6-dichloro-1,4,5,8-naphthalene tetracarboxylic diimide (NTCDI-Cl_2-$(CH_2C_3F_7)_2$) are investigated. High-voltage NTCDI-Cl_2-$(CH_2C_3F_7)_2$ TFTs already showed electron mobilities up to 1.3 cm^2/Vs.[17]

Initially, organic TFTs were fabricated on doped Si substrates with a 30-nm-tick global Al back-gate. The gate dielectric consists of 3.6-nm-thick plasma-grown AlO_x and a 1.7-nm-thick self-assembled monolayer of n-tetradecylphosphonic acid, enabling low-voltage operation due to its high areal capacitance (800 nF/cm^2).[18] On the gate dielectric, nominally 20 nm of the organic semiconductor NTCDI-Cl_2-$(CH_2C_3F_7)_2$ (Fig. 1(a)) were deposited by vacuum sublimation at a substrate temperature of 50 °C and a deposition rate of 0.3 Å/s. Figs. 1(b) and 1(c) show terraced layers with step heights of about 2 nm which is close to the length of the molecule,[16] indicating that the molecules are standing approximately upright. Finally, 25-nm-thick gold source/drain contacts were evaporated through high-resolution silicon stencil masks. All electrical measurements were performed in air at room temperature.

Fig. 2 shows the transfer (drain-source voltage $V_{DS} = 1.5$ V) and output characteristics (gate-source voltage V_{GS} up to 3 V) of a TFT with a channel width of $W = 50$ μm, a channel length of $L = 1$ μm, and a contact length (overlap between source/drain contact and gate electrode) of $L_C = 200$ μm. The TFT has a maximum effective field-effect mobility of 0.06 cm^2/Vs, an on/off current ratio of 10^6, a

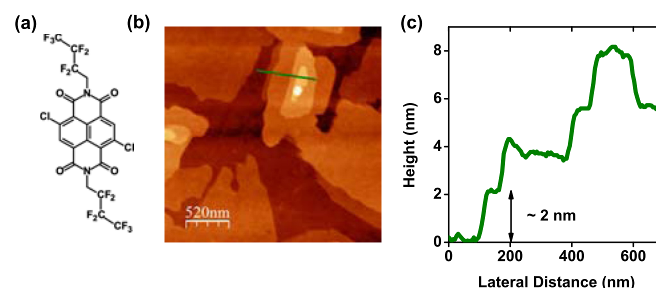

FIG. 1. (a) Chemical structure of NTCDI-Cl_2-$(CH_2C_3F_7)_2$. (b) AFM image of a nominally 20-nm-thick vacuum-deposited NTCDI-Cl_2-$(CH_2C_3F_7)_2$ film. (c) Height profile of the section marked in Fig. 1(b).

a)Electronic mail: R.Roedel@fkf.mpg.de

 © 2013 AIP Publishing LLC

Downloaded 13 Jun 2013 to 134.105.156.141. This article is copyrighted as indicated in the abstract. Reuse of AIP content is subject to the terms at: http://apl.aip.org/about/rights_and_permissions

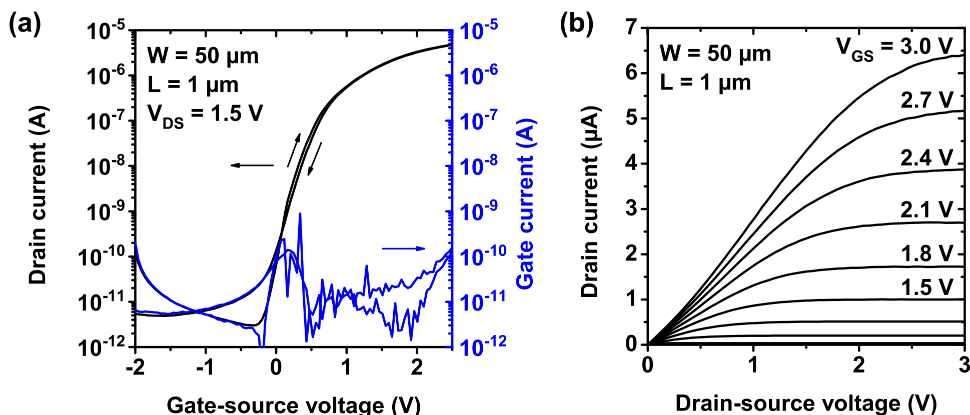

FIG. 2. Current-voltage characteristics of an organic n-channel TFT with a channel length of 1 μm, measured under ambient conditions. (a) Transfer curve. (b) Output curve.

subthreshold swing of 180 mV/decade, a threshold voltage of 0.3 V, a transconductance of 60 mS/m, and minimal hysteresis. The small value of the effective mobility is due to the short channel length at which the contact resistance dominates over the channel resistance. In Fig. 3(a), the dependence of the effective mobility on the channel length in the linear regime is shown, demonstrating an increase up to 0.8 cm^2/Vs for a channel length of 100 μm.

From the simple equation,[19] $\mu_{eff} = \mu_0 R_{ch}/(R_C + R_{ch})$ with the effective field-effect mobility μ_{eff}, the intrinsic field-effect mobility μ_0 (free of contact effects), the contact resistance R_C and the channel resistance R_{ch}, the channel-length dependence of the effective mobility can be formulated as

$$\mu_{eff} = \frac{\mu_0}{1 + \frac{L_{1/2}}{L}}, \tag{1}$$

where $L_{1/2}$ is a characteristic channel length at which the contact resistance and the channel resistance are equal. Using μ_0 and $L_{1/2}$ as fitting parameters, the measured effective mobilities in Fig. 3(a) can be properly reproduced by Eq. (1). The fit gives an intrinsic mobility of 1.5 cm^2/Vs and $L_{1/2} = 85$ μm.

A more general approach to determine the intrinsic transistor properties is the transmission line method (TLM)[20] which considers the total resistance of transistors with different channel lengths measured directly at a fixed overdrive voltage $V_{GS} - V_{th}$. In the linear regime, the total resistance R_{tot} can be expressed in terms of the channel length by

$$R_{tot}W = R_C W + \frac{L}{\mu_0 C_i (V_{GS} - V_{th})}, \tag{2}$$

where C_i is the areal gate-dielectric capacitance and V_{th} is the threshold voltage, here extracted by the second derivative method.[21] TLM is strictly valid only if the contact resistance is independent of V_{DS}. The slight nonlinearity seen in Fig. 2(b) at small V_{DS} indicates a small dependence of the contact resistance on V_{DS}, an observation that is supported by V_{DS}-dependent contact resistance measurements on a different sample (not shown). However, since this effect is very small, it can be safely ignored here. Plotting $R_{tot}W$ as a function of L, the width-normalized contact resistance $R_C W$ and the intrinsic mobility μ_0 can be extracted from the y-axis intercept and the slope of the linear fit, respectively. This is demonstrated in Fig. 3(b) for different gate overdrive voltages at $V_{DS} = 0.1$ V. For a gate overdrive voltage of 1.6 V, the fit provides a width-normalized contact resistance of 4.7 kΩ cm and an intrinsic electron mobility of 1.4 cm^2/Vs. For high-performance p-channel TFTs fabricated with the same device architecture, but using dinaphtho[2,3-b:2′,3′-f]thieno[3,2-b]thiophene (DNTT) as the semiconductor, values of $R_C W = 0.6$ kΩ cm and $\mu_0 = 3$ cm^2/Vs were obtained under similar measurement conditions.[6] It can be seen that the performance of our n-channel TFTs approaches that of high-performance p-channel devices, even though the contact resistance is somewhat larger in the n-channel TFTs, probably due to the less favorable line-up of the energy levels usually found at the contact/semiconductor interfaces in organic n-channel

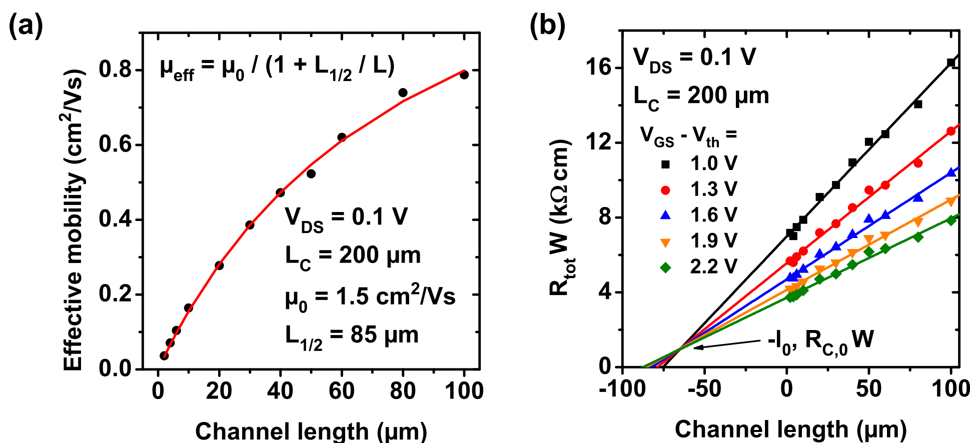

FIG. 3. (a) Effective field-effect mobility of TFTs with a contact length of 200 μm as a function of the channel length at $V_{DS} = 0.1$ V. The red line is a fit according to Eq. (1). (b) Width-normalized total resistance as a function of the channel length for different gate overdrive voltages. All linear fit curves meet at a single point which defines a characteristic length $l_0 = 64$ μm and a characteristic width-normalized resistance $R_{C,0}W = 1$ kΩ cm.

Downloaded 13 Jun 2013 to 134.105.156.141. This article is copyrighted as indicated in the abstract. Reuse of AIP content is subject to the terms at: http://apl.aip.org/about/rights_and_permissions

transistors compared with optimized p-channel TFTs.[22] For DNTT (HOMO of −5.4 eV)[23] and NTCDI-Cl_2-($CH_2C_3F_7$)$_2$ (LUMO of −4 eV),[16] the nominal energy barriers are 0.4 eV and 1 eV assuming a work function of gold of around 5 eV.[24,25] The real values are probably altered by effects like interface dipoles, surface contamination and diffusion of the contact metal into the semiconductor.[26,27]

In staggered TFT architectures, the area contributing to charge injection must be considered carefully. The model commonly known as current crowding describes the contact regions as resistor networks where the effective injection area is the result of a balance between the vertical resistances (contact resistivity ρ_C) and the sheet resistance R_{sheet} of the channel.[28,29] This defines the transfer length L_T, which is the effective length over which most of the charge carriers are exchanged between the contacts and the semiconductor,

$$L_T = \sqrt{\frac{\rho_C}{R_{sheet}}}. \quad (3)$$

For long contact lengths ($L_C \gg L_T$), Berger[28] has shown that the dependence of the total resistance on the channel length can then be expressed as

$$R_{tot}W = \frac{L + 2L_T}{\mu_0 C_i (V_{GS} - V_{th})}, \quad (4)$$

so the transfer length can be extracted by extrapolating the total resistance to the x-axis in Fig. 3(b). In addition, the contact resistivity ρ_C can be calculated by

$$\rho_C = (R_C W)^2 \mu_0 C_i (V_{GS} - V_{th})/4. \quad (5)$$

Fig. 4 shows the dependence of several extracted transistor parameters on the gate overdrive voltage. While the intrinsic mobility and the transfer length show only little variation with values of around $\mu_0 = 1.35$ cm^2/Vs and $L_T = 40\,\mu$m, the contact resistance and contact resistivity both significantly decrease with increasing gate overdrive voltage. The observation that the contact resistance decreases with increasing gate overdrive voltage can be explained as follows: A higher gate overdrive voltage induces a greater density of accumulated charges in the channel and thereby decreases the sheet resistance which constitutes the horizontal part of the contact resistance. A reduced sheet resistance makes a greater contact area available for charge transfer and consequently reduces the contact resistance. This would be true even if the contact resistivity was not affected by the gate overdrive voltage. However, our measurements indicate that the contact resistivity, i.e., the vertical part of the contact resistance, also decreases with increasing gate overdrive voltage, even though there is no direct dependence between the contact resistivity and the sheet resistance. This observation can be explained as follows: A higher gate overdrive voltage induces not only a greater carrier density in the channel, but also a significant tail of charge carriers in the bulk of the semiconducting film, thereby reducing the bulk resistivity originating from the vertical charge transport through the semiconductor between the source/drain contacts and the channel.[30,31] The large observed variation of the contact resistivity with the gate overdrive voltage indicates a significant contribution of the bulk resistivity if the resistivity of the contact-semiconductor interface is assumed to depend only weakly on the gate overdrive voltage.

In Fig. 3(b), the linear fits for the various gate overdrive voltages all cross at a single point. Based on this fact, Luan *et al.* proposed an empirical model where the width-normalized contact resistance is composed of a constant part $R_{C,0}W$ in series with an accumulation layer characterized by the length l_0 and the mobility μ,[32]

$$R_C W = R_{C,0} W + \frac{l_0}{\mu C_i (V_{GS} - V_{th})}. \quad (6)$$

In order to illustrate that the curve indeed shows a linear dependence, we plot in Fig. 4(c) the contact resistance as a function of the inverse gate overdrive voltage. Using $l_0 = 64\,\mu$m and $R_{C,0}W = 1$ kΩ cm extracted from the intersection point in Fig. 3(b), the data can be properly fitted by Eq. (6) with $\mu = 1.33$ cm^2/Vs. Due to the charge accumulation in the bulk semiconductor,[30] the contact resistivity ρ_C also depends linearly on the inverse gate overdrive voltage, with the axis intercept $\rho_{C,0} = 4\,\Omega\,$cm^2.

As shown in Fig. 5(a), the transistors have a good stability in air. The fact that the electron mobility was still above 0.3 cm^2/Vs after these TFTs had been stored in a cleanroom under ambient conditions for about seven months probably originates from the low LUMO energy of NTCDI-Cl_2-($CH_2C_3F_7$)$_2$ of about −4 eV (Ref. 16) that helps to resist ambient oxidation.[33] Another factor is the kinetic barrier created

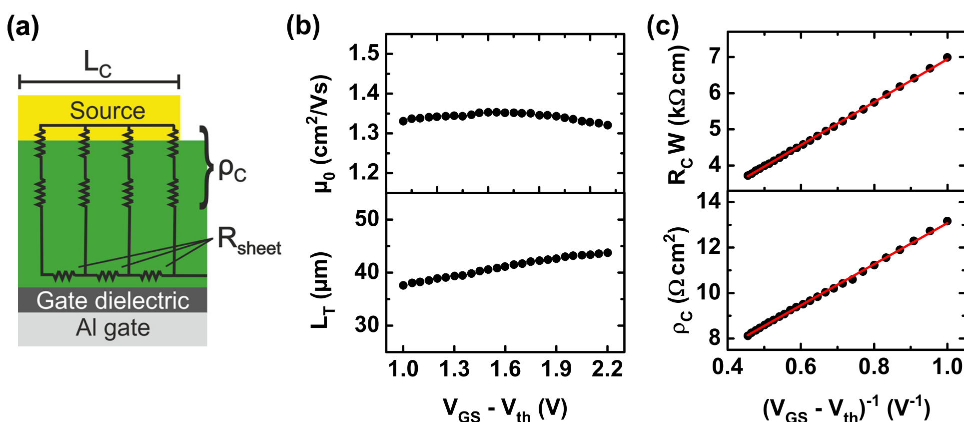

FIG. 4. (a) Schematic of the source side of the TFT, illustrating the different resistances. (b) Intrinsic mobility (top) and transfer length (bottom) as a function of the gate overdrive voltage. (c) Width-normalized contact resistance (top) and contact resistivity (bottom) as a function of the inverse gate overdrive voltage. The red lines are linear fits.

Downloaded 13 Jun 2013 to 134.105.156.141. This article is copyrighted as indicated in the abstract. Reuse of AIP content is subject to the terms at: http://apl.aip.org/about/rights_and_permissions

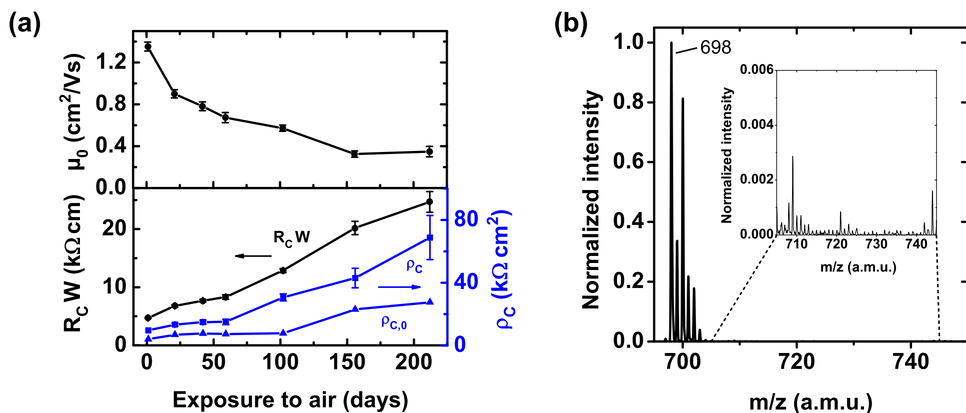

FIG. 5. (a) Evolution of TFT parameters during air exposure at a gate overdrive voltage of 1.6 V. Top: Intrinsic electron mobility. Bottom: Width-normalized contact resistance (black circles), contact resistivity (blue squares), and constant part of the contact resistivity $\rho_{C,0}$ (blue triangles). The errors are taken from the standard error of the linear fit of R_{tot} vs. L. (b) Mass spectrum of a NTCDI-Cl_2-$(CH_2C_3F_7)_2$ film after about 14 months in air. No oxidation products are visible. Inset: Magnification of the region where oxidation products would be expected.

by the dense packing of the fluorocarbon chains[16] in combination with the hydrophobicity of the semiconducting layer (contact angle 126°) that hinder the penetration of water molecules into the channel. While the intrinsic mobility was still about one quarter of the initial value after seven months in air, the contact resistance had increased by a factor of around five and the contact resistivity and its constant part $\rho_{C,0}$ had increased by a factor of seven. This is surprising, since from a degradation of the intrinsic semiconductor mobility alone, the contact resistance and contact resistivity would be expected to increase with at most the same rate, even if the mobility in the semiconductor regions below (and protected by) the metal contacts degrades with the same rate as in the (unprotected) channel region. The fact that the increase in contact resistance and resistivity is slightly faster than the drop of the intrinsic mobility indicates that there is an additional degradation path for the contact resistance.

The nature of the degradation mechanism is unclear. For pentacene, De Angelis *et al.* have observed oxidation products by mass spectroscopy at additional masses of +15 amu and +16 amu (and multiples) that are believed to cause the observed mobility degradation in that material by producing trap states.[34] However, mass spectra of a thin NTCDI-Cl_2-$(CH_2C_3F_7)_2$ film taken after about 14 months in air using laser desorption ionization time-of-flight mass spectrometry (LDI-TOF-MS) show only negligible intensity in the mass range where oxidation products would be expected (Fig. 5(b)), so the observed reduction of the mobility does not seem to be caused by oxidation of the semiconductor molecules.

All electrical measurements shown so far were performed on the same sample. The statistics of fresh devices obtained together with TFTs of seven other samples fabricated in the same way over a period of more than four months are presented in Fig. 6. For unknown reasons, three of the samples show a somewhat higher contact resistance, but most samples have a low contact resistance below 10 kΩ cm. The mean intrinsic mobility is (0.85 ± 0.27) cm^2/Vs.

In order to evaluate the dynamic performance of the TFTs, we fabricated 11-stage organic complementary ring oscillators based on NTCDI-Cl_2-$(CH_2C_3F_7)_2$ (n-channel) and DNTT (p-channel).[18] In contrast to the devices described above, the ring oscillators were fabricated on a flexible polyethylene naphthalate (PEN) substrate with local Al gate electrodes and Au interconnects, using in total five different stencil masks to pattern the various layers.

The signal propagation delay per stage τ was calculated as $\tau = 1/2fn$ with the measured oscillation frequency of the ring oscillators f and the number of stages $n = 11$. Fig. 7(a) shows τ as a function of the supply voltage V_{DD} for three different ring oscillators that are comprised of TFTs with channel lengths of 4, 2, and 1 μm and contact lengths of 20, 10, and 5 μm. In order to account for the difference in the effective hole and electron mobilities, the channel width of the n-channel TFTs ($W = 80\ \mu$m) was chosen to be larger than that of the higher-mobility p-channel TFTs ($W = 40\ \mu$m).

As the channel and contact lengths are reduced, the parasitic capacitances decrease, resulting in shorter propagation delays. As expected,[35] the frequency of the ring oscillators is proportional to the supply voltage (inset of Fig. 7(a)).

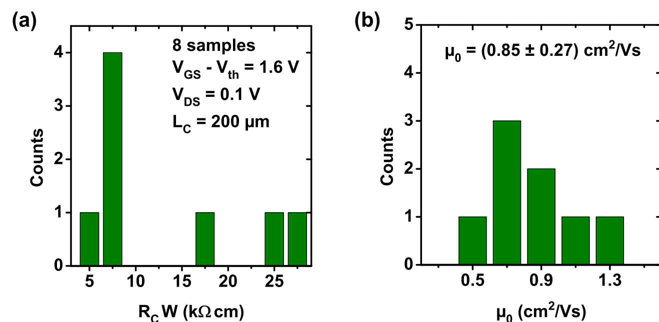

FIG. 6. (a) Statistics of the width-normalized contact resistance extracted from 8 samples fabricated under the same conditions. (b) Statistics of the intrinsic mobility for 8 samples. The mean value is (0.86 ± 0.23) cm^2/Vs.

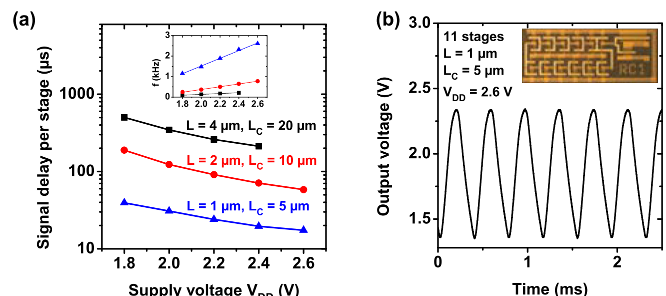

FIG. 7. (a) Stage delay of flexible 11-stage organic complementary ring oscillators based on NTCDI-Cl_2-$(CH_2C_3F_7)_2$ (n-channel) and DNTT (p-channel) as a function of the supply voltage. The lines are guides to the eye. Inset: Oscillation frequency of the ring oscillators as a function of the supply voltage. The straight lines illustrate the linear relationship. (b) Output signal of the ring oscillator with a channel length of 1 μm and a contact length of 5 μm at a supply voltage of 2.6 V. Inset: Photograph of the complementary ring oscillator.

Downloaded 13 Jun 2013 to 134.105.156.141. This article is copyrighted as indicated in the abstract. Reuse of AIP content is subject to the terms at: http://apl.aip.org/about/rights_and_permissions

For a supply voltage of 2.6 V, the output signal of the ring oscillator with a channel length of 1 μm and a contact length of 5 μm is shown in Fig. 7(b). The signal delay per stage is 17 μs, which is the lowest value reported for organic complementary ring oscillators at low supply voltages ($<$10 V). For supply voltages above 10 V, the shortest signal delays of flexible organic complementary ring oscillators were reported by Smaal *et al.*[36] (10 μs at 20 V) and by Baeg *et al.*[35] (1.25 μs at 30 V).

In summary, we have presented n-channel organic thin-film transistors with low-voltage operation, high mobility, small contact resistance and air stability. TFTs with channel lengths down to 1 μm have been fabricated, revealing a strong influence of the contact resistance. A detailed analysis of the contact resistance shows good agreement with existing models and significant contributions of the bulk semiconductor resistivity. Although the value of the contact resistance is relatively low and approaching that of p-channel transistors, it still severely limits the device performance at small channel lengths. Organic complementary ring oscillators on a flexible substrate with different channel and contact lengths were fabricated. A signal delay per stage as low as 17 μs was measured, which is the lowest reported value for an organic complementary ring oscillator at supply voltages below 10 V.

This work was funded by BASF SE, the German Ministry of Education and Research (project POLYTOS; FKZ: 13N10205, 13N12084; Research Network Forum Organic Electronics) and the German Research Foundation (DFG) under Grant KL 2223/5-1. The authors would like to thank DuPont Teijin Films for providing the PEN substrates.

[1]S. C. B. Mannsfeld, B. C. K. Tee, R. M. Stoltenberg, C. V. H. H. Chen, S. Barman, B. V. O. Muir, A. N. Sokolov, C. Reese, and Z. Bao, Nature Mater. **9**, 859 (2010).
[2]T. Someya, Y. Kato, T. Sekitani, S. Iba, Y. Noguchi, Y. Murase, H. Kawaguchi, and T. Sakurai, Proc. Natl. Acad. Sci. U.S.A. **102**, 12321 (2005).
[3]K. Myny, S. Steudel, S. Smout, P. Vicca, F. Furthner, B. van der Putten, A. K. Tripathi, G. H. Gelinck, J. Genoe, W. Dehaene, and P. Heremans, Org. Electron. **11**, 1176 (2010).
[4]I. Yagi, N. Hirai, Y. Miyamoto, M. Noda, A. Imaoka, N. Yoneya, K. Nomoto, J. Kasahara, A. Yumoto, and T. Urabe, J. Soc. Inf. Disp. **16**, 15 (2008).
[5]G. H. Gelinck, H. Huitema, E. van Veenendaal, E. Cantatore, L. Schrijnemakers, J. van der Putten, T. Geuns, M. Beenhakkers, J. Giesbers, B. Huisman, E. J. Meijer, E. M. Benito, F. J. Touwslager, A. W. Marsman, B. J. E. van Rens, and D. M. de Leeuw, Nature Mater. **3**, 106 (2004).
[6]F. Ante, D. Kälblein, T. Zaki, U. Zschieschang, K. Takimiya, M. Ikeda, T. Sekitani, T. Someya, J. N. Burghartz, K. Kern, and H. Klauk, Small **8**, 73 (2012).
[7]U. Zschieschang, M. J. Kang, K. Takimiya, T. Sekitani, T. Someya, T. W. Canzler, A. Werner, J. Blochwitz-Nimoth, and H. Klauk, J. Mater. Chem. **22**, 4273 (2012).
[8]D. Bode, K. Myny, B. Verreet, B. van der Putten, P. Bakalov, S. Steudel, S. Smout, P. Vicca, J. Genoe, and P. Heremans, Appl. Phys. Lett. **96**, 133307 (2010).
[9]M. Kitamura, Y. Kuzumoto, S. Aomori, and Y. Arakawa, Appl. Phys. Express **4**, 051601 (2011).
[10]B. K. Crone, A. Dodabalapur, R. Sarpeshkar, R. W. Filas, Y. Y. Lin, Z. Bao, J. H. ONeill, W. Li, and H. E. Katz, J. Appl. Phys. **89**, 5125 (2001).
[11]M. M. Ling and Z. Bao, Org. Electron. **7**, 568 (2006).
[12]H. E. Katz, J. Johnson, A. J. Lovinger, and W. Li, J. Am. Chem. Soc. **122**, 7787 (2000).
[13]B. A. Jones, M. J. Ahrens, M. H. Yoon, A. Facchetti, T. J. Marks, and M. R. Wasielewski, Angew. Chem. Int. Ed. **43**, 6363 (2004).
[14]H. Yan, Z. Chen, Y. Zheng, C. Newman, J. R. Quinn, F. Dötz, M. Kastler, and A. Facchetti, Nature **457**, 679 (2009).
[15]Y. Zhao, C. Di, X. Gao, Y. Hu, Y. Guo, L. Zhang, Y. Liu, J. Wang, W. Hu, and D. Zhu, Adv. Mater. **23**, 2448 (2011).
[16]J. H. Oh, S. L. Suraru, W. Y. Lee, M. Könemann, H. W. Höffken, C. Röger, R. Schmidt, Y. Chung, W. C. Chen, F. Würthner, and Z. Bao, Adv. Funct. Mater. **20**, 2148 (2010).
[17]M. Stolte, S. L. Suraru, F. Würthner, J. H. Oh, Z. Bao, J. Brill, M. Könemann, J. Qu, U. Zschieschang, and H. Klauk, Proc. SPIE **7778**, 777804 (2010).
[18]U. Zschieschang, F. Ante, D. Kälblein, T. Yamamoto, K. Takimiya, H. Kuwabara, M. Ikeda, T. Sekitani, T. Someya, J. Blochwitz-Nimoth, and H. Klauk, Org. Electron. **12**, 1370 (2011).
[19]M. Marinkovic, D. Belaineh, V. Wagner, and D. Knipp, Adv. Mater. **24**, 4005 (2012).
[20]D. Natali and M. Caironi, Adv. Mater. **24**, 1357 (2012).
[21]D. Boudinet, G. L. Blevennec, C. Serbutoviez, J.-M. Verilhac, H. Yan, and G. Horowitz, J. Appl. Phys. **105**, 084510 (2009).
[22]C. R. Newman, C. D. Frisbie, D. A. da Silva Filho, J. L. Brédas, P. C. Ewbank, and K. R. Mann, Chem. Mater. **16**, 4436 (2004).
[23]T. Yamamoto and K. Takimiya, J. Am. Chem. Soc. **129**, 2224 (2007).
[24]P. A. Anderson, Phys. Rev. **115**, 553 (1959).
[25]H. B. Michaelson, J. Appl. Phys. **48**, 4729 (1977).
[26]H. Peisert, M. Knupfer, and J. Fink, Appl. Phys. Lett. **81**, 2400 (2002).
[27]C. Shen and A. Kahn, J. Appl. Phys. **90**, 4549 (2001).
[28]H. H. Berger, J. Electrochem. Soc. **119**, 507 (1972).
[29]D. Schroder, *Semiconductor Material and Device Characterization* (Wiley, 2006).
[30]T. J. Richards and H. Sirringhaus, J. Appl. Phys. **102**, 094510 (2007).
[31]C. Tanase, E. J. Meijer, P. W. M. Blom, and D. M. De Leeuw, Org. Electron. **4**, 33 (2003).
[32]S. Luan and G. W. Neudeck, J. Appl. Phys. **72**, 766 (1992).
[33]B. A. Jones, A. Facchetti, M. R. Wasielewski, and T. J. Marks, J. Am. Chem. Soc. **129**, 15259 (2007).
[34]F. De Angelis, M. Gaspari, A. Procopio, G. Cuda, and E. Di Fabrizio, Chem. Phys. Lett. **468**, 193 (2009).
[35]K.-J. Baeg, S.-W. Jung, D. Khim, J. Kim, D.-Y. Kim, J. B. Koo, J. R. Quinn, A. Facchetti, I.-K. You, and Y.-Y. Noh, Org. Electron. **14**, 1407 (2013).
[36]W. Smaal, C. Kjellander, Y. Jeong, A. Tripathi, B. van der Putten, A. Facchetti, H. Yan, J. Quinn, J. Anthony, K. Myny, W. Dehaene, and G. Gelinck, Org. Electron. **13**, 1686 (2012).

Downloaded 13 Jun 2013 to 134.105.156.141. This article is copyrighted as indicated in the abstract. Reuse of AIP content is subject to the terms at: http://apl.aip.org/about/rights_and_permissions